



## Tele-impedance based assistive control for a compliant knee exoskeleton



Nikos Karavas<sup>a,\*</sup>, Arash Ajoudani<sup>a,b</sup>, Nikos Tsagarakis<sup>a</sup>, Jody Saglia<sup>a</sup>, Antonio Bicchi<sup>a,b</sup>, Darwin Caldwell<sup>a</sup>

<sup>a</sup> Istituto Italiano di Tecnologia, Italy

<sup>b</sup> Interdepartmental Research Centre “E. Piaggio”, University of Pisa, Italy

### HIGHLIGHTS

- We propose a tele-impedance based assistive control for a knee exoskeleton.
- An EMG-driven biomechanical model estimates the net torque and joint stiffness trend index.
- The outputs of the model are used to derive the trajectory and stiffness of the exoskeleton's impedance controller.
- The exoskeleton can generate assistive actions that are volitionally controlled by the user's muscle activity.

### ARTICLE INFO

*Article history:*  
Available online 16 October 2014

*Keywords:*  
Lower limb exoskeleton  
Assistive robotics  
Impedance control  
Stiffness augmentation

### ABSTRACT

This paper presents a tele-impedance based assistive control scheme for a knee exoskeleton device. The proposed controller captures the user's intent to generate task-related assistive torques by means of the exoskeleton in different phases of the subject's normal activity. To do so, a detailed musculoskeletal model of the human knee is developed and experimentally calibrated to best match the user's kinematic and dynamic behavior. Three dominant antagonistic muscle pairs are used in our model, in which electromyography (EMG) signals are acquired, processed and used for the estimation of the knee joint torque, trajectory and the stiffness trend, in real time. The estimated stiffness trend is then scaled and mapped to a task-related stiffness interval to agree with the desired degree of assistance. The desired stiffness and equilibrium trajectories are then tracked by the exoskeleton's impedance controller. As a consequence, while minimum muscular activity corresponds to low stiffness, i.e. highly transparent motion, higher co-contractions result in a stiffer joint and a greater level of assistance. To evaluate the robustness of the proposed technique, a study of the dynamics of the human-exoskeleton system is conducted, while the stability in the steady state and transient condition is investigated. In addition, experimental results of standing-up and sitting-down tasks are demonstrated to further investigate the capabilities of the controller. The results indicate that the compliant knee exoskeleton, incorporating the proposed tele-impedance controller, can effectively generate assistive actions that are volitionally and intuitively controlled by the user's muscle activity.

© 2014 Elsevier B.V. All rights reserved.

### 1. Introduction

Powered exoskeletons have undergone continuous technological development over the past few years and have found various applications from military use to patient rehabilitation. Military exoskeletons' purpose is to augment the soldier's muscular force

and endurance in carrying heavy loads [1]. On the other hand, rehabilitation exoskeletons aim at recovering the neuromusculoskeletal function of stroke or post-surgical patients [2–4], while assistive exoskeletons can assist elderly or individuals with mobility disorders during demanding, in terms of power, motion tasks [5–7].

Independently from the use, exoskeletons are robotic devices that are worn by the humans. Therefore, the application of forces in an appropriate manner as regards the timing, magnitude, direction and location on the human body, is a prerequisite [8]. In other words, the exoskeleton should effectively assist the natural human motion ensuring the safety and comfort of the user, and

\* Correspondence to: Harvard University, 60 Oxford Street, Suite 403, 02138 Cambridge, MA, United States.

E-mail address: [nkaravas@seas.harvard.edu](mailto:nkaravas@seas.harvard.edu) (N. Karavas).

that his/her agility is not deteriorated. To address this immense challenge researchers have incorporate the detection of the user's intent into the control of exoskeletons. Common approach is to use joint angles to infer about the subject's posture [9], or ground reaction forces measurements to estimate the desired torques with an inverse dynamic model [1]. In [10] authors proposed an observer to correct the desired joint torques computed from the ground reaction forces. However, due to the increased need in exoskeletons for achieving desired response to disturbance, the integration of biological signals into the exoskeleton control has gained a lot of attention by many researchers over the last decade [6,11,12].

Furthermore, as exoskeletons not simply cooperate with the humans but assist or supplement the human motion (e.g. replace muscle's work), it has been deemed imperative to develop exoskeletons that exhibit biological behavior and performance [13]. This is mainly related to the physical properties of the musculotendinous unit acting on the human joints and their resultant impedance. In particular, several biomechanical studies of human movement report that the impedance profiles of the human joints vary substantially during motion [14,15]. Therefore, exoskeletons should accordingly respond and adapt to these impedance profiles [16]. In this manner, their use becomes more effective and intuitive, while the agility and comfort of the user wearing the device are significantly increased.

To this end, researchers have put a lot of effort into employing variable impedance systems into exoskeletons, orthoses or prostheses that will be able to produce naturally human-like mechanics [17,18]. However, the planning of the impedance profiles of these devices has been deemed a highly challenging task and yet relies on indirect approaches such as modeling, gait phase detection, or off-line learning and optimization techniques. For instance, in [19] the active impedance of an ankle orthosis is modulated during the gait cycle using a finite-state machine that is triggered by ground reaction forces and joint angles. Additionally, the authors in [20] select to adjust the knee joint impedance of an assistive exoskeleton during motion with the target stiffness, damping and inertia parameters being identified based on the Recursive Least Square (RLS) method. Furthermore, variable-impedance assistance has been implemented in robot-aided gait rehabilitation to achieve patient-cooperative training and more interactive robotic therapies, that lead to an enhanced rehabilitation outcome [21,22]. In the latter an adaptive impedance controller utilizes an inverse-dynamics based estimation of the user's torque in order to adapt robotic assistance.

Alternatively to these approaches, which are constrained either by highly nonlinear models [20,22] or by optimization criteria problems [23], in this series of preliminary case studies we propose to select and control the impedance of the exoskeleton joint based on real-time stiffness measurements of the corresponding human joint. The current manuscript is an extended and enriched version of the initial work in [24] to provide an exhaustive analysis and discussion especially on the proposed control scheme and its experimental evaluation. Particular attention is paid to the dynamics of the physical human-exoskeleton system, the performance of the controller in the frequency domain, and the stability of the closed-loop system both in steady state and time-varying condition.

The presented control method requires modeling of musculoskeletal bio-feedbacks such as muscular forces-moments. This can be addressed with two general approaches. Inverse dynamic methods, investigate this problem by means of measurements of the joint positions and applied external forces. However, several drawbacks are attributed to such techniques [25]. For instance, the muscles acting on each joint are grouped and divided to agonist and antagonist blocks and consequently, the external flexion and

extension moments are balanced. Therefore, these methods are not reliable enough for individual estimation of muscular forces since a priori assumptions are made on the role of individual muscles during the optimization of a predefined cost function [26]. The problem grows when modeling complex tasks which combine highly nonlinear muscle activation and contraction dynamics and geometry variations. As a result, a second group of general solutions which are associated with forward dynamic approaches have been proposed. In these methods, neural commands are extracted and fed to the detailed neuro-musculoskeletal model of the limbs [27].

Therefore, an EMG-driven musculoskeletal model of the knee joint has been developed that blends results of different biomechanical studies. The outputs of the model are then exploited in real-time by the impedance controller implemented in the exoskeleton joint. Regarding the hardware, a knee exoskeleton was used for this study that is a passively compliant device demonstrating inherently soft interaction based on the series elastic actuation (SEA) principle [2,8]. We envisage this assistive device combined with the proposed control to assist either individuals with limited physical capabilities (e.g. elderly) during their activities of daily living, or healthy people during repetitive tasks at work for reducing their average muscle forces. However, the presented control algorithm could be eventually used under conditions (i.e. sound muscle excitations) in a rehabilitation setting for improved patient-driven therapies.

The rest of the paper is structured as follows. Section 2 presents the musculoskeletal model of the knee joint while Section 3 discusses the knee model identification and calibration. Section 4 describes the exoskeleton hardware and Section 5 introduces the tele-impedance based assistive control scheme. Section 6 discusses the dynamics of the physical system and the stability of the proposed control, while Section 7 demonstrates the experimental trials. Moreover, Section 8 provides a general discussion on this work and Section 9 addresses the conclusions.

## 2. EMG-driven musculoskeletal model

This section describes mathematically the electromyography-driven musculoskeletal model of the human knee joint, which is used to account for the net torque and joint stiffness trend index. Three antagonistic muscle groups (six muscles) which are denoted as being the dominant surface muscles acting on the knee joint were chosen in order to form the presented musculoskeletal model. Fig. 1 illustrates the anatomy of the thigh muscles and the placement of the electrodes. In particular, six electrodes (Bagnoli-16, Delsys Inc.) were attached to the extensor [rectus femoris (RF), vastus medialis (VM) and vastus lateralis (VL)] and flexor [biceps femoris (BF), semimembranosus (SM) and semitendinosus (ST)] muscles. Furthermore, for the reader's convenience in Fig. 2 is depicted an overview of the adopted model structure which consists of the muscle activation dynamics, muscle contraction dynamics and musculoskeletal geometry sections. As shown, from the processed electromyography of each muscle  $u_i$  are derived the muscle activations  $a_i$  and then the muscle-tendon forces  $F_i^{mt}$  which result in the net torque  $\tau_{net}$  and the knee joint stiffness trend  $STI$ .

### 2.1. Activation dynamics

Electromyography (EMG) signals inherit patterns of activations of involved muscles. In order to extract muscular activations, the raw EMG signals must be processed. First, these signals are high-pass filtered to remove offsets and movement artifacts. This stage is followed by full rectification techniques [28]. Consequently, the resulting signals are low-pass filtered and normalized in order to provide traces of the neural activation of the muscles. In



**Fig. 1.** Front and rear view of the human thigh illustrating the selected six muscles (three antagonistic groups) whose electromyography was used for the musculoskeletal modeling.

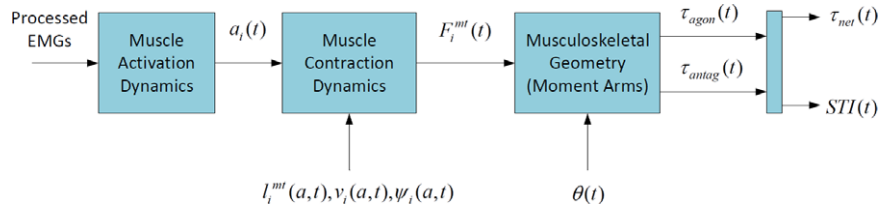


**Fig. 2.** Block diagram of the information flow within the musculoskeletal model for deriving the net torque and the stiffness trend index.

this manuscript, the processed electromyographic signal of each muscle is denoted as  $u_i(t)$ .

Concerning the motor unit level, it has been observed that muscle force variations with respect to neural commands demonstrate an exponential trend [29]. As a result, activation of the muscles  $a_i$  is defined by:

$$a_i(t) = \frac{e^{A u_i(t)} - 1}{e^A - 1} \quad (1)$$

where  $-3 < A < 0$  is a nonlinear shape factor.

## 2.2. Contraction dynamics

Large scale modeling of the muscular force arising from activation dynamics is widely performed based on Hill's muscle model [30] and its extension proposed by Zajac [27]. These models are well-established in the biomechanics literature [29], and have been extensively exploited in assistive technologies where there exists human–robot interaction [12,31,32]. In such cases, the muscle–tendon unit is modeled as a muscle fiber in series with a viscoelastic tendon (see Fig. 3). Muscle fiber itself is modeled by a contractile element in parallel with an elastic component. The general equation associating the force generated by the contractile element with the muscle–tendon force  $F_i^{mt}(t)$  reads as follows:

$$F_i^{mt}(t) = F_i^{max} [f_i(l) f_i(v) a_i(t) + f_{p_i}(l)] \cos(\psi_i(t)) \quad (2)$$

where  $F_i^{mt}(t) = F_i^t(t)$ , with  $F_i^t$ ,  $f_i(l)$ ,  $f_i(v)$  corresponding to the tendon force, normalized force–length and normalized force–velocity curves of the contractile element of muscle number  $i$ , and  $f_{p_i}$  refers to the passive elastic normalized force–length relation (see details in [27] and [29]). The pennation angle, which is defined as the angle between the tendon and the muscle fibers, is denoted by  $\psi_i(t)$  and can be given by the following equation:

$$\psi_i(t) = \sin^{-1} \left( \frac{l_i^{mt} \sin(\psi_{o_i})}{l_i^m(t)} \right) \quad (3)$$

where  $l_i^m(t)$  is the muscle fiber length and  $\psi_{o_i}$  the pennation angle at the optimal muscle fiber length  $l_{o_i}^m$ .

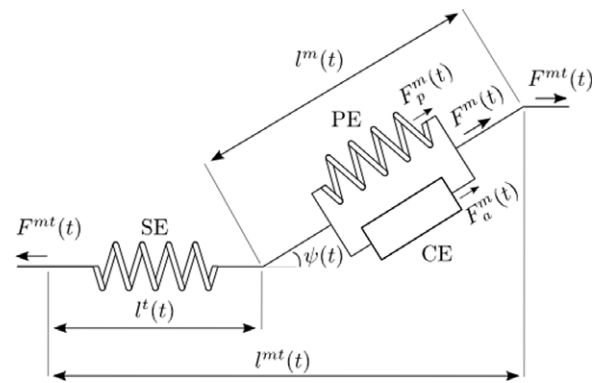


**Fig. 3.** Representation of the muscle–tendon unit based on Hill's model.

Huijing in [33] has observed that the optimal muscle fiber length increases as the muscle activation decreases. To take into account this dependency of optimal muscle fiber length on activation fluctuations we adopt the relationship introduced in [29]:

$$l_{o_i}^m(t) = l_{o_i}^m (\gamma (1 - a_i(t)) + 1) \quad (4)$$

where  $l_{o_i}^m$  represents the optimal fiber length at maximum activation and  $\gamma$  is the percentage change in optimal fiber length, chosen to be 15% [29].

A dense body of literature reports on the linear relationship between the tendon slack length  $l_s^t$ , tendon force and the tendon length  $l^t$ . Such mapping is shown to be valid for  $l^t > l_s^t$  [25,29]. Here, similar assumptions have been made in modeling the tendon length. In addition, we can write:

$$l_i^t(t) = l_i^{mt}(t) - l_i^m(t) \cos(\psi_i(t)) \quad (5)$$

with  $l^{mt}$  denoting the muscle–tendon length.

## 2.3. Musculoskeletal geometry

The lengths of the muscle–tendon complexes acting on the knee joint are shown to be functions of the knee joint angle [34]. In these works, the muscle length values were fitted to a second order

polynomial by means of least squares optimization technique. Consequently,  $\bar{l}_i^{mt}(t)$  which accounts for the percentage of segment length (the origin-to-insertion length relative to its length in full extension of the knee) is defined and identified as follows:

$$\bar{l}_i^{mt}(t) = C_{0_i} + C_{1_i}\theta_{knee}(t) + C_{2_i}\theta_{knee}^2(t) \quad (6)$$

where  $\theta_{knee}$  represents the knee joint angle in degrees and  $C_{0_i}$ ,  $C_{1_i}$  and  $C_{2_i}$  are constants (see [34] for details). By adopting (4), (5) and (6) the muscle fiber length can be identified and used for the estimation of the contraction dynamics. Note that, as far as concerns the accuracy of the model parameters of the muscle fiber of each muscle we rely on the previous biomechanics studies [25,29,34] and the re-identification experiment that is described in Section 3.

The muscle moment arms  $r_i(t)$  of the muscle–tendon unit can be described based on the displacements method proposed in [35] which is defined by:

$$r_i(t) = \frac{\partial \bar{l}_i^{mt}(t)}{\partial \theta_{knee}} \quad (7)$$

Consequently, the moment arms are determined as follows:

$$\bar{r}_i(t) = [C_{1_i} + 2C_{2_i}\theta_{knee}(t)] \frac{180}{\pi} \quad (8)$$

where moment arms  $\bar{r}_i(t)$  are expressed as a percentage of segment length.

Once we have estimated the forces (2) and the moment arms (8) of all chosen muscles acting on the joint, we are able to convert the muscle forces to joint torques  $\tau$  by means of the following equation:

$$\tau(t) = \left| \sum_{i=1}^n \tau_i(t) \right|_{agonist} - \left| \sum_{j=1}^k \tau_j(t) \right|_{antagonist} \quad (9)$$

where  $\tau_i(t) = F_i(t)r_i(t)$ ,  $\tau_j(t) = F_j(t)r_j(t)$  with  $n$  and  $k$  being the number of agonist and antagonist muscles acting on the joint, respectively.

It has been shown that a simultaneous increase in antagonistic muscle torques acting on the joint, does not affect the joint torque (as seen in (9)) although it does increase joint stiffness [36]. Therefore, we can define the stiffness trend index (STI) as:

$$STI(t) = \left| \sum_{agonist} \tau_i(t) \right| + \left| \sum_{antagonist} \tau_j(t) \right| \quad (10)$$

and the stiffness of the knee joint as:

$$K(t) = \alpha \times STI(t) + \beta \quad (11)$$

where  $\alpha$  ( $\text{rad}^{-1}$ ) and  $\beta$  ( $\text{Nm/rad}$ ) are to be identified constants.

### 3. Model identification–calibration

Several caveats apply to the forward dynamic methods, described in Section 2. To begin with, concerning the EMG signals, one must take into account reliable post-processing techniques in order to maximize robustness of the estimation of muscular activations. For instance, day-to-day and subject to subject variations, temperature and humidity fluctuations, electrode misplacement, crosstalk between signals and movement artifacts will give rise to inaccuracy and drift of the estimated signals. Furthermore, the model parameters ((2)–(6)) vary among subjects.

To minimize the modeling uncertainty, the parameters of the model must be re-identified based on each user’s experimental data. For this reason, we have set up identification–calibration experiments to re-identify the parameters as described below.

#### 3.1. Calibration experiments

One healthy subject (male, 27 years old) participated in identification–calibration experiments. The raw EMG signals were processed (at 1 kHz) and the muscular activities were estimated during the identification experiments as well as during the tele-impedance control experiments that are to be described in Section 7.

The initial values of the model parameters as presented in Section 2 were extracted from the literature [25,26,30–35]. In order to choose the number of parameters to be re-identified, one must consider the reasonable tradeoff between modeling uncertainty and identification complexity. Hence, seven constant parameters of each muscle referring to the activation and contraction dynamics and muscle–tendon geometry were chosen to be adjusted relying on identification experiments. The chosen parameters were: the maximum isometric muscle fiber force  $F^{max}$ , the pennation angle at optimal fiber length  $\psi_o$ , the optimal fiber length  $l_o^m$ , the nonlinear shape factor  $A$ , and the constants  $C_0$ ,  $C_1$  and  $C_2$ .

For the identification experiments the subject was wearing the knee exoskeleton while having the EMG electrodes attached as it was described in Section 2 and illustrated in Fig. 1. In order to take into account the muscle activation of both the knee flexor and the extensor in the model identification, we performed two tasks that involved each of the antagonistic group of muscles separately. The exoskeleton was commanded to provide torques that were proportional to the angular displacement from the equilibrium position (active stiffness control). During the first task the subject assumed a stand posture while the equilibrium position of the exoskeleton was set to  $0^\circ$ . The subject was instructed to flex his right knee at a certain angle with the minimum possible contraction (flexor contribution). For every two trials the exoskeleton stiffness was varying with a varied step as shown in Table 1 resulting in 20 trials. During the second task the subject was seated and the equilibrium position of the exoskeleton was set to  $90^\circ$ , while he was asked to repeatedly extend his knee with minimum contraction as well (extensor contribution). For each two trials the exoskeleton stiffness was increased from 0 to 200 Nm/rad with a varied step similarly with the first task, see Table 1. Thus, this task resulted in additional 20 trials.

During this experiment the torque applied by the human  $\hat{\tau}_h$  can be estimated by the following equation:

$$\hat{\tau}_h = J\ddot{\theta}_{knee} + D\dot{\theta}_{knee} + \tau_g + \tau_e \quad (12)$$

where  $J$  represents the total inertia of the shank and the exoskeleton’s lower segment,  $D$  denotes the damping of the human knee and the exoskeleton joint, while  $\tau_g$  is the gravitational torque applied on the coupled system. In addition,  $\tau_e$  is the torque applied by the exoskeleton and equals to the measured elastic torque  $\tau_s$ . Note that movements were carried out at very low knee angular velocity and acceleration (quasi static). For this reason, the inertial and damping moment effects were negligible in our setup and were not taken into consideration. Thus, (12) can be simplified as:

$$\hat{\tau}_h = \tau_e + \tau_g = \tau_s + (m_{sh} + m_{lseg})gl_{CoM} \sin(\theta_{knee}) \quad (13)$$

where  $m_{sh}$  denotes the mass of shank,  $m_{lseg}$  is the mass of the lower segment of the exoskeleton and  $l_{CoM}$  refers to the center of mass of the combined lower link and shank.

Even trials were chosen for the identification while the odd ones were kept for evaluative analysis of the identification procedure. The six-channel processed EMGs data together with the torques  $\hat{\tau}_h$  and  $\tau_e$  were used to identify the musculoskeletal model parameters, described in 2. Due to the nonlinear dependency between the knee joint torque and the corresponding muscular activities, a nonlinear least square algorithm is utilized for the identification of the model parameters while being constrained to  $\pm 10\%$  above/below of their nominal values.

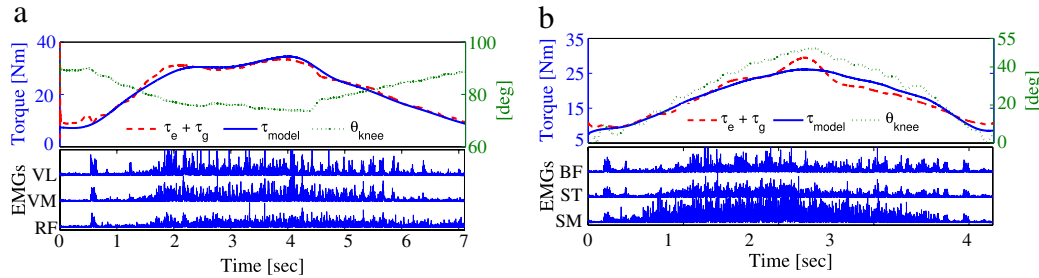


**Fig. 4.** Comparison of the estimated torque of the knee joint and the one derived from the musculoskeletal model in extension (a) and flexion (b) identification trials. Knee angular positions are also given, while in the lower plots are depicted the full rectified EMGs of the contributing muscles.

**Table 1**  
Experimental Protocol used for the Model Calibration.

Number of trial	Exoskeleton EQ (deg)	Exoskeleton stiffness (Nm/rad)	Number of trial	Exoskeleton EQ (deg)	Exoskeleton stiffness (Nm/rad)
1&2 (flexion)	0°	0	21&22 (extension)	90°	0
3&4 (flexion)	0°	10	23&24 (extension)	90°	10
5&6 (flexion)	0°	20	25&26 (extension)	90°	20
7&8 (flexion)	0°	30	27&28 (extension)	90°	30
9&10 (flexion)	0°	40	29&30 (extension)	90°	40
11&12 (flexion)	0°	50	31&32 (extension)	90°	50
13&14 (flexion)	0°	60	33&34 (extension)	90°	60
15&16 (flexion)	0°	100	35&36 (extension)	90°	100
17&18 (flexion)	0°	150	37&38 (extension)	90°	150
19&20 (flexion)	0°	200	39&40 (extension)	90°	200

### 3.2. Model validation

Typical results of the validation of the identified model using extension and flexion test trials are demonstrated in Figs. 4(a) and 4(b), respectively. These experiments were performed with the exoskeleton stiffness being set at 30 Nm/rad. The upper plots show the model net torque  $\tau_{model}$  and the measured torque  $\tau_e$ , including the gravitational part  $\tau_g$ . The position of the knee joint  $\theta_{knee}$  as it was measured by the exoskeleton is also depicted in the upper plots. Lower plots of the figures demonstrate the corresponding full rectified EMG signals of the dominant muscles. To evaluate the accuracy of the model, the normalized root mean square error (NRMSE) was calculated for each test trial as follows:

$$NRMSE = \frac{\sqrt{\frac{\sum_{i=1}^n (\tau_{model}(i) - \tau_{measured}(i))^2}{n}}}{\tau_{measured_{max}} - \tau_{measured_{min}}} \quad (14)$$

with  $n$  denoting the number of points in each trial, and  $\tau_{measured} = \tau_g + \tau_e$ . The resulting values then were averaged for all the test trials (extension and flexion) resulting in an average value of 12.4%. This error, even acceptable, comes partly from the modeling uncertainty in our musculoskeletal model and partly from the neglected effects of inertia and damping in  $\tau_{measured}$ . Future work will investigate model identification methods that will include also dynamic movements.

### 4. Knee exoskeleton description

Physical human–robot interaction requires devices that present fast adaptation to human volitional actions and safe behavior during unexpected impacts [37]. To achieve these, it is essential that the exoskeleton actuation system demonstrates low output mechanical impedance and high force fidelity. In this context, series elastic actuators (SEA) have been introduced to drive robots and subsequently implemented into exoskeletons [2,8]. In these actuation systems, an elastic element is placed between the motor and the load and acts as an energy buffer. This lowers the loop

**Table 2**  
Specifications of CompAct-RS.

Description	Symbol	Value	Unit
Max Cont. Output Power	$P_{Rated}$	209	Watts
Elastic Torque (Max)	$\tau_s$	80	Nm
Motor Torque (Max)	$\tau_M$	1.53	Nm
Elastic deflection (Max)	$\theta_s$	11	deg
Elastic energy (Max)	$U_s$	5.5	J
Allowable stiffness range	$K_S$	200 ~ 800	Nm/rad

gain of the closed-loop system allowing for increased control gains while still remaining within the stability margins [38]. High control gains improve significantly robustness to changing loads and tolerance to impacts, while lower the output impedance. Therefore, SEA allow for precise and robust force control which plays a key role to impedance-controlled systems.

The assistive device that was used for this pilot study is a lightweight knee exoskeleton that is powered by CompAct-RS [39, 40]. CompAct-RS is a rotational series elastic actuator which is able to reconfigure offline its apparent stiffness  $K_S$  to achieve subject-specific and task-specific compliance levels. Table 2 shows the specifications of CompAct-RS. For this work, this was set to  $K_S = 200$  Nm/rad, that was suitable for the execution of the experiments which are described in Sections 3 and 7. As mentioned above, a significant benefit of the inserted elasticity is that it can be used for robust torque sensing by measuring the springs deflection with a high resolution optical encoder (AEDA 3300, Avago Technologies). This allows to achieve precise torque control and avoid the addition of a conventional load cell that is expensive and delicate. Nevertheless, the series elastic element affects the dynamics of the overall system and, as it will be described in Section 6, it needs to be included in the pertinent analysis.

Fig. 5 shows a subject wearing the exoskeleton on his right leg with the axis of rotation of the exoskeleton joint aligned with the axis of the user's knee joint. The exoskeleton interfaces with the wearer by means of four rigid braces and is fastened with four Velcro straps at thigh and shank. The location of the bracing points can be adjusted along the structure to accommodate different leg sizes. Particular attention was paid to fast and easy donning and

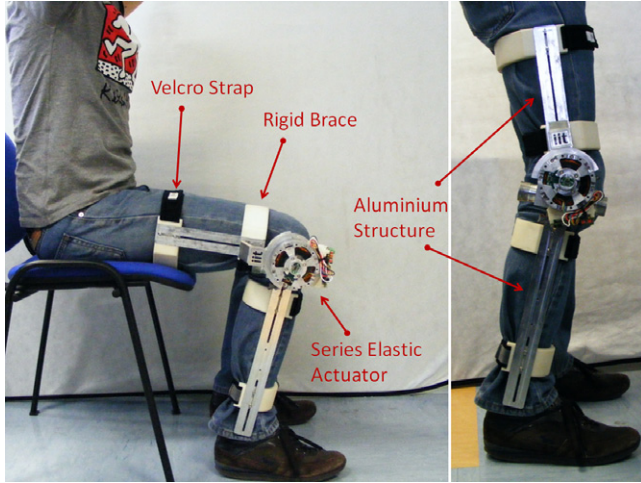


Fig. 5. The inherently compliant knee exoskeleton actuated by the series elastic actuator CompAct-RS.

doffing (estimated less than one minute). Moreover, the range of motion of the knee exoskeleton in the sagittal plane is between 0° and 120° where 0° corresponds to full extension of the knee. Mechanical limits ensure that the actuator operates within this motion range and ensures the exoskeleton safe to use.

### 5. Tele-impedance based assistive control

An ideal assistive device should generate supporting forces upon the user’s request and simultaneously present high levels of transparency during no assistance condition [8]. This implies that it should match the performance of humans in terms of displacement and impedance regulation over a wide range of loads and motions [41,42]. In some extent we address this challenge by exploiting tele-impedance, an approach that aims at replicating stiffness regulation skills of humans to robots [43]. In particular, the exoskeleton is able to provide stiffness augmentation to the user on the basis of his/her stiffness trace with the purpose of achieving effective assistance when is needed and to present high levels of compliance when the muscle activation of the user is low. Regarding tele-impedance, it was previously proposed during tele-operated tasks which require significant dynamics variation as an alternative method to unilateral position based control or bilateral force reflecting control. The algorithm provides the robot with task-related stiffness profile in addition to position–orientation trajectories [44].

The tele-impedance based proposed method utilizes electromyography as the primary basis. In contrast with other proposed EMG-based techniques implemented in exoskeletons [6,32], that perform proportional torque control using the estimated user’s torque, here we select to control in real-time the active impedance of the exoskeleton according to stiffness estimates of the user’s joint. Hence, we exploit the improved robustness of the impedance control over the pure torque control due to its ability to keep the desired joint configuration, even if the torque sensing/control is imperfect [45]. Moreover, we avoid other limitations reported in studies with torque amplification-based exoskeletons, where small variations in the estimated user’s torque cause undesirable high accelerations during high amplification ratios [32].

To produce tele-impedance control we utilize the EMG-driven biomechanical model that was described in Section 2 and a common impedance controller implemented in the exoskeleton’s actuator unit. Hence, the exoskeleton tracks a torque reference signal  $\tau_{ref}$  that is governed by the virtual impedance  $G_c$  and is given

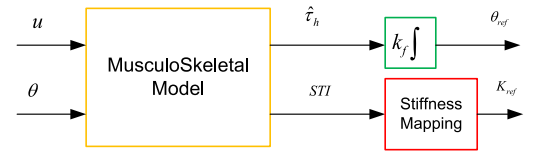


Fig. 6. Diagram that illustrates the derivation of the reference signals of the impedance controller from the musculoskeletal model.

by the following equation:

$$\tau_{ref} = K_c(\theta_{ref} - \theta_e) + B_c(\dot{\theta}_{ref} - \dot{\theta}_e) \quad (15)$$

where  $K_c$ ,  $B_c$  represent the stiffness and the damping parameters of the virtual impedance of reference, respectively. In addition  $\theta_e$  and  $\theta_{ref}$  denote the exoskeleton’s motor position and its reference position, respectively. Fig. 6 depicts the derivation of the references signals of the impedance controller (i.e.  $K_{ref}$ ,  $\theta_{ref}$ ) from the musculoskeletal model. In particular, the model uses as inputs the processed EMGs and the knee angle  $q$  and outputs the estimated user torque  $\hat{\tau}_h$  and the stiffness trend index  $STI$ .

#### Stiffness mapping

The stiffness reference input for the knee exoskeleton is obtained from (11). The stiffness trend index (STI) is mapped to a desired stiffness range that is defined according to the task and subject requirements. For instance, when the subject is during high load condition the exoskeleton provides motion assistance, while when he/she acts during low load condition (i.e. no assistance is required) the exoskeleton is transparent and does not impede the user’s motion. In this manner, the exoskeleton can mimic the biological stiffness function and respond to the user’s voluntary motions. Furthermore, in case of disabled individuals different levels of stiffness augmentation can be applied depending on the particular motion task and subject. Thus, the identification of  $\alpha$  and  $\beta$  in Eq. (11) is task-related and subject-specific. In this manuscript, the desired stiffness range is determined experimentally based on a desired assistance performance (see Section 7).

A critical aspect when designing assistive control strategies is also the detection of the user’s intended motion. In this work, we infer about the user’s movement using the estimated user torque  $\hat{\tau}_h$ . In particular, to generate assistive torques in the direction of motion we select to update the equilibrium position of the knee exoskeleton joint in accordance with the user’s intended motion, the equilibrium of which is obtained from the estimated user torque  $\hat{\tau}_h$  using the following formula:

$$\theta_{ref} = \begin{cases} k_f \int (\hat{\tau}_h - a) dt & \hat{\tau}_h > a \\ 0 & -a < \hat{\tau}_h < a \\ k_f \int (\hat{\tau}_h + a) dt & \hat{\tau}_h < -a \end{cases} \quad (16)$$

where  $k_f$  and  $a$  are the sensitivity constant and the noise dead band constant, respectively.

As is illustrated in Fig. 7, the controller is composed of an inner torque loop and an outermost position loop. The position and stiffness references described above feed the equilibrium position and the active stiffness of the tele-impedance controller, respectively. The active damping is set to vary proportionally to the active stiffness as  $B_c = bK_c = 0.01K_c$ . By deriving the equilibrium position of the controller from (16), assistive forces augment the user’s desired actions/motions via the virtual impedance  $G_c$ . Note that, the controller operates at 1 kHz which is also the sampling frequency of the EMGs.

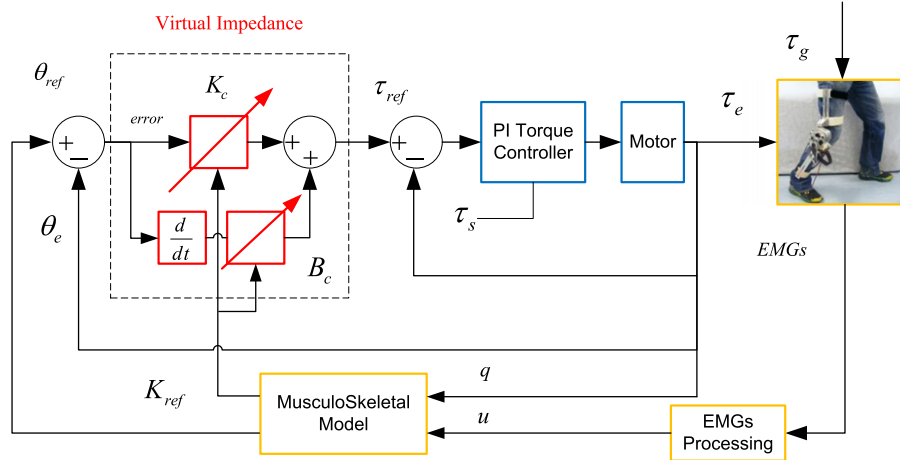


Fig. 7. The implemented tele-impedance controller that utilizes the EMG-driven musculoskeletal model.

## 6. The human–exoskeleton system dynamics for the standing-up motion

To evaluate the effectiveness of the assistance provided to the subject and the operation of the proposed control technique, we select to study the standing up motion, which is one of the most demanding task in terms of torque and power for the knee joint. Hence, the model of the closed-loop human–exoskeleton system during standing-up is presented below. The system's response in the time and frequency domain are investigated, while its stability is analyzed within the usable range of the active stiffness  $K_c$ . As the active stiffness varies in real-time the stability should be investigated also under this dynamic condition and the allowable maximum rate of the impedance regulation that ensures stability has to be identified. To authors knowledge there is no such a study to address this matter (i.e. stability of active impedance control systems) mainly due to the high complexity of the pertinent systems.

### 6.1. System modeling

A simplified human body model with 1-DOF in the sagittal plane coupled with the knee exoskeleton is considered. In Fig. 8 is illustrated the human body model and the signals flow of the tele-impedance controller. As shown, for the sake of simplicity the masses of the thigh, pelvis and torso have been combined into a single body of mass  $m_h$ . This obviously affects the estimation of the gravitational loads during motion. However, assuming a concentrated inertia (i.e. no torso motion) can be deemed as a worst-case scenario in terms of knee torque, since it has been observed that humans incline forward their trunks during standing-up in order to decrease the gravitational load and hence, facilitate the task [6]. Moreover, the ankle and foot dynamics have been neglected (i.e shank is considered to be fixed to the ground) as during standing-up slight ankle motion has been reported [46]. The external torques acting on the system are the exoskeleton's actuator torque  $\tau_e$ , the human net torque  $\tau_h$  and the gravitational torque  $\tau_g$ . During the sitting to standing transition the system motion can be described by the following equation:

$$\mathbf{M}\ddot{\mathbf{x}} + \mathbf{B}\dot{\mathbf{x}} + \mathbf{K}\mathbf{x} + \mathbf{G} = \boldsymbol{\tau} \quad (17)$$

where  $\mathbf{M} = \text{diag}(I_h, I_e) \in \mathbb{R}^{2 \times 2}$  with  $I_e$  being the reflected motor inertia after the reduction drive. Moreover,  $\mathbf{B} \in \mathbb{R}^{2 \times 2}$  is the damping matrix,  $\mathbf{K} \in \mathbb{R}^{2 \times 2}$  is a symmetric stiffness matrix, and  $\mathbf{G} \in \mathbb{R}^{2 \times 1}$  is the gravity vector.  $\mathbf{x} \in \mathbb{R}^{2 \times 1}$  and  $\boldsymbol{\tau} \in \mathbb{R}^{2 \times 1}$  refer to the position

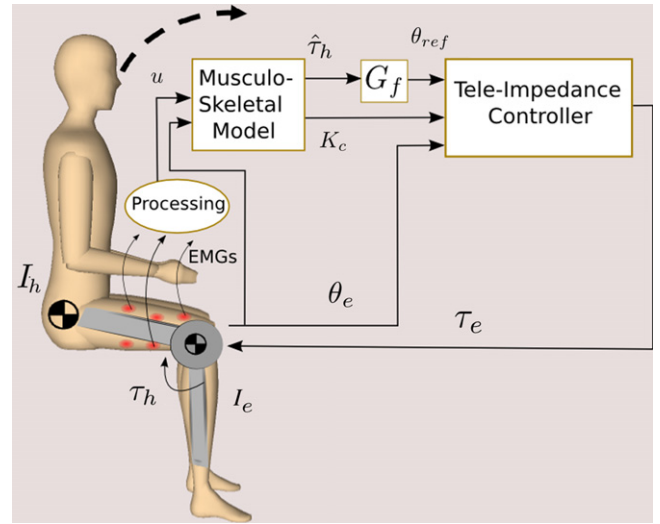


Fig. 8. Representation of the simplified physical system of the human-knee-exoskeleton and the concept of the tele-impedance control.

and torque vector, respectively. Eq. (17) can be rewritten in matrix form as follow:

$$\begin{bmatrix} I_h & 0 \\ 0 & I_e \end{bmatrix} \begin{bmatrix} \ddot{q} \\ \dot{\theta}_e \end{bmatrix} + \begin{bmatrix} B_h & 0 \\ 0 & B_e \end{bmatrix} \begin{bmatrix} \dot{q} \\ \dot{\theta}_e \end{bmatrix} + \begin{bmatrix} K_S & -K_S \\ -K_S & K_S \end{bmatrix} \begin{bmatrix} q \\ \theta_e \end{bmatrix} = \begin{bmatrix} \tau_h - m_h g l \sin q \\ \tau_e \end{bmatrix} \quad (18)$$

where  $\theta_e = \frac{\theta_m}{N}$ ,  $\dot{\theta}_e = \frac{\dot{\theta}_m}{N}$  are the position and velocity of the exoskeleton motor, respectively reflected at the link side after the gear reduction ( $N = 100:1$ ). As already mentioned,  $K_S$  denotes the series elasticity of the actuator. The inertia of the human body is calculated as  $I_h = m_h l^2$ , where  $l$  refers to the distance from the knee joint center to the center of the combined human body mass. In addition,  $I_e = N^2 J_m$  denotes the reflected motor inertia after the reduction drive, while  $B_e = N^2 B_m$  is the damping of the exoskeleton motor reflected also after the reduction drive.  $q$  and  $\dot{q}$  refer to the position and velocity of the knee joint. Fig. 9 depicts a schematic representation of (18) for the convenience of the reader.

### 6.2. System response analysis

To study the operational concept of the tele-impedance based assistive control and the system's response both in time and

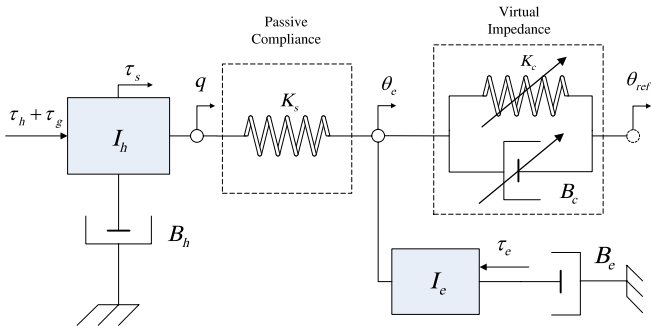


**Fig. 9.** Conceptual schematic that illustrates the interaction mechanics between exoskeleton and human including the tele-impedance controller.

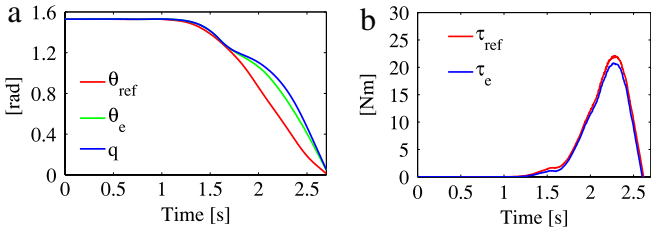


**Fig. 10.** Simulation results corresponding to the standing-up motion.

frequency domain, simulations were conducted on the 1-DOF system that was modeled in Section 6.1.

As inputs of the model (Eq. (18)) were used the estimated torque  $\hat{\tau}_h$  and the reference stiffness  $K_{ref}$ , that were recorded during the experiment described in Section 7, since they cannot be simulated. Additionally, the combined mass of the human body was set as  $M_h = 60$  kg. The viscous damping of the knee joint varies significantly with muscle contraction and knee flexion angle and is reported to be within the range 1–5 Nms/rad [47]. Based on these findings the damping of the human knee joint was selected to be in the middle of this range, thus  $B_h = 2.5$  Nms/rad. The motor inertia and damping both reflected after the reduction drive were  $I_e = 0.36$  kgm<sup>2</sup> and  $B_e = 0.607$  Nms/rad, while the active damping was set to  $B_c = 0.01K_c$ . The sensitivity constant was selected at  $k_f = 0.034$ , a value that was tuned during the experimental trials in Section 7.

Fig. 10(a) shows the motion of the knee  $q$  towards the reference position  $\theta_{ref}$  and the deflection  $\theta_s = \theta_e - q$  of the elastic element which allows the transmission of the assistive torque from the actuator’s motor to the knee joint. The exoskeleton torque tracking of  $\tau_{ref}$  is shown in Fig. 10(b).

The frequency response of the closed-loop system is also discussed. The coupled pair (human leg + exoskeleton device) described in Section 6.1 can be described in the frequency domain by the following equations:

$$(G_h + G_s)X_h = \tau_h + \tau_g + G_s X_e \quad (19)$$

$$(G_e + G_s)X_e = N\tau_m + G_s X_h \quad (20)$$

where  $X_h = \mathcal{L}[q(t)]$  and  $X_e = \mathcal{L}[\theta_e(t)]$  with  $\mathcal{L}$  symbolizing the Laplace operator. The combined human body is modeled as a second order linear impedance:  $G_h = I_h s^2 + B_h s$ . Additionally,  $G_s = K_s$  represents the series elasticity between the motor and the output link and  $G_e = I_e s^2 + B_e s$  models the mass and damping properties of the motor.

If we assume that the motor can track the reference torque perfectly, it can be written:

$$\tau_m = G_c(X_{eq} - X_e) \quad (21)$$

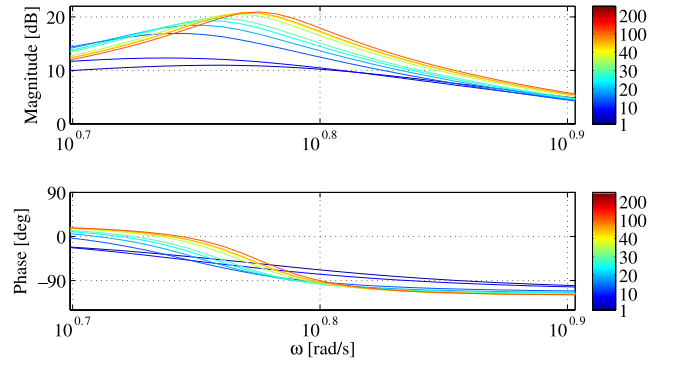


**Fig. 11.** Zoomed Bode plots of the transfer function  $\frac{X_h}{X_e}$  for different values of the active stiffness  $K_c$  (side colorbars depict values of  $K_c$  in Nm/rad).

where  $G_c = K_c + B_c s$  is the virtual impedance of the controller and  $X_{eq} = \mathcal{L}[\theta_{ref}(t)]$ . As mentioned in Section 5, the reference position is derived from the estimated user torque as:

$$X_{eq} = G_f \tau_h \quad (22)$$

where  $G_f = k_f/s$ .

Inserting (22) into (21), substituting  $\tau_m$  in (20) and then substituting  $\tau_h$  in (19), while rearranging with respect to  $X_h$  gives:

$$X_h = \frac{NG_f G_c + NG_c + G_{es}}{G_f G_{es} G_{hs} + NG_f G_c G_{hs} - G_f G_s^2} X_e + \frac{NG_c + G_{es}}{G_{es} G_{hs} + NG_c G_{hs} - G_s^2} \tau_g \quad (23)$$

where  $G_{hs} = G_h + G_s$  and  $G_{es} = G_e + G_s$  are used only for simplifying the equation.

Having the transfer function  $\frac{X_h}{X_e}$  the frequency response of the closed-loop system can be investigated. This is done within a range of the active stiffness  $K_c$  close to the one which was applied during the experiments described in Section 7. Fig. 11 demonstrates the Bode plots of the  $\frac{X_h}{X_e}$  dynamics for different values of  $K_c$ . For demonstration purposes the magnitude and phase plots are shown only for the frequency range in which sort of variation is present. The inherent elasticity was set at  $K_s = 200$  Nm/rad. As shown, considerable changes of the resonant peak occur within the small range of  $0 < K_c < 30$  Nm/rad. Moreover, the peak of the magnitude of the transfer function varies from 10 to 20 dB for the entire range of  $1 < K_c < 200$  Nm/rad, while for  $K_c > 35$  Nm/rad it does not demonstrate any significant variation being close to 20 dB.

By neglecting the furthest away pole pair with respect to the imaginary axis, we can approximate the system using a second-order equation. Omitting the nonlinear effect of the gravity is safe though, as this analysis is focused on the performance evaluation of the tele-impedance controller in terms of system response while the active stiffness  $K_c$  and series elasticity  $K_s$  are varying. Thus, the natural frequency  $\omega_n$  and the damping ratio  $\zeta$  of the second-order closed loop system were calculated for different values of the active stiffness  $K_c$  and the series elasticity  $K_s$  and are depicted in Fig. 12. As shown, both the natural frequency  $\omega_n$  and the damping ratio  $\zeta$  do not vary significantly when the stiffness of the virtual impedance,  $K_c$  is changing. This is due to the fact that the value of the active stiffness  $K_c$  does not have much affect on the dominant pole pair of the transfer function  $\frac{X_h}{X_e}$ . On the other hand, as expected we can notice a significant change of the natural frequency  $\omega_n$  and the damping ratio  $\zeta$  as the stiffness of the series elasticity  $K_s$  decreases. Hence, it is evident that the dynamics of the system are mainly affected by the series elasticity and not by the active stiffness. This means that the system’s response depends on the mechanical compliance of the exoskeleton’s actuator rather than the regulation of the tele-impedance controller.

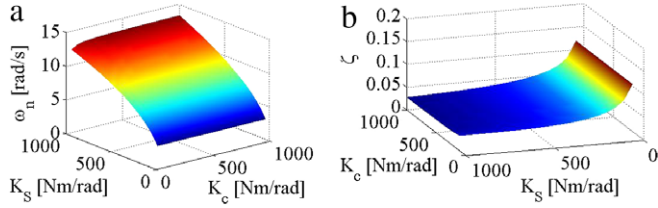


Fig. 12. Natural frequency (a) and damping ratio (b) for different values of  $K_c$  and  $K_s$ .

### 6.3. Stability analysis for time-variant virtual spring–damper

As the main feature of the proposed tele-impedance control scheme is the real-time variation of the active impedance based on the stiffness estimates of the user's knee joint, the behavior of the system in terms of stability has to be examined not only in the steady state condition but also during the transient state. Another important matter is the maximum allowable rate, with which the active stiffness  $K_c$  can vary ensuring the stability of the closed-loop system. In this subsection both of these concerns will be investigated using the quadratic stability theory for continuous-time systems with polytopic uncertainties [48].

**Theorem 1.** Consider the following linear continuous-time parameter-varying polytopic system:

$$\begin{aligned} \dot{\mathbf{x}}(t) &= (\xi_1 \mathbf{A}_1 + \xi_2 \mathbf{A}_2 + \dots + \xi_k \mathbf{A}_k) \mathbf{x}(t) \\ &= \mathbf{A}_{\sigma(t)} \mathbf{x}(t) \end{aligned} \quad (24)$$

where  $\mathbf{x} \in R^n$  is the state vector,  $\mathbf{A}_m \in R^{n \times n}$ ,  $m = 1, 2, \dots, k$  are constant matrices and  $\xi = [\xi_1 \dots \xi_k] \in R^k$  is a vector of uncertain, possibly time varying parameters with  $\sum_{i=1}^k \xi_i = 1$  and  $0 \leq \xi_i \leq 1$ .  $k$  is the number of the polytope vertices. The uncertain system (24) is quadratically stable if and only if there exists a positive definite matrix  $\mathbf{P}_{\sigma}$  such as:

$$\mathbf{A}_{\sigma} \mathbf{P}_{\sigma} + \mathbf{A}_{\sigma}^T \mathbf{P}_{\sigma} < 0. \quad (25)$$

In our case the only time-varying variable of the system is  $K_c$ , as the damping parameter is proportional to the stiffness  $K_c$ . Hence, the vertices  $\mathbf{A}_{\sigma}$  can be written as follows:

$$\begin{cases} \mathbf{A}_1 = \mathbf{A}_0 + \mathbf{A}_{var}[K_{c_{max}}] \\ \mathbf{A}_2 = \mathbf{A}_0 + \mathbf{A}_{var}[K_{c_{min}}] \end{cases} \quad (26)$$

where  $\mathbf{A}_0$  is a constant matrix and  $\mathbf{A}_{var}(K_c)$  is the time-varying matrix. Thus, according to the above theorem the system is quadratically stable if and only if there exists a positive definite  $\mathbf{P}$  that satisfies the following LMIs (Linear Matrix Inequality) condition:

$$\begin{cases} \mathbf{A}_1^T \mathbf{P} + \mathbf{A}_1 \mathbf{P} < 0 \\ \mathbf{A}_2^T \mathbf{P} + \mathbf{A}_2 \mathbf{P} < 0. \end{cases} \quad (27)$$

By calculating  $\mathbf{A}_1$  and  $\mathbf{A}_2$  the quadratic stability of the system (24) can be investigated easily using the *quadstab* function of MATLAB, which seeks a positive definite  $\mathbf{P}$  that establishes quadratic stability. In addition, quadratic stability also allows infinitely fast rate of change in the parameters because the solution  $\mathbf{P}$  to the LMIs (27) is a constant matrix [49].

For this study the equilibrium position is set to be zero, therefore the control law is described as follow:

$$\tau_e = -K_c \theta_e - B_c \dot{\theta}_e = -K_c \theta_e - b K_c \dot{\theta}_e. \quad (28)$$

In addition, the human net torque is an external signal and does not affect the stability analysis, thus  $\tau_h = 0$ . By substituting (28)

into (17), that describes the physical system, and by considering the approximation  $\sin q \approx q$ , it can be written:

$$\mathbf{M}\ddot{\mathbf{x}} + \mathbf{B}\dot{\mathbf{x}} + \mathbf{K}\mathbf{x} = \mathbf{G}\mathbf{x} + \mathbf{K}_c \mathbf{x} + \mathbf{B}_c \dot{\mathbf{x}} \quad (29)$$

where  $\mathbf{G}$  is the linear gravity matrix:

$$\mathbf{G} = \begin{bmatrix} -mgl & 0 \\ 0 & 0 \end{bmatrix} \quad (30)$$

while  $\mathbf{K}_c$  and  $\mathbf{B}_c$  refer to the active stiffness and damping matrices, respectively and are given by the following equations:

$$\mathbf{K}_c = \begin{bmatrix} 0 & 0 \\ 0 & -K_c \end{bmatrix}, \quad \mathbf{B}_c = \begin{bmatrix} 0 & 0 \\ 0 & -bK_c \end{bmatrix}. \quad (31)$$

Eq. (29) can be rewritten in the form:

$$\begin{aligned} \ddot{\mathbf{x}} &= -\mathbf{M}^{-1} \mathbf{B} \dot{\mathbf{x}} - (\mathbf{M}^{-1} \mathbf{K} - \mathbf{M}^{-1} \mathbf{G}) \mathbf{x} \\ &\quad + \mathbf{M}^{-1} \mathbf{K}_c \mathbf{x} + \mathbf{M}^{-1} \mathbf{B}_c \dot{\mathbf{x}}. \end{aligned} \quad (32)$$

By setting:

$$\mathbf{z} = \begin{bmatrix} \mathbf{x} \\ \dot{\mathbf{x}} \end{bmatrix} \quad (33)$$

(32) becomes as follow:

$$\dot{\mathbf{z}} = \mathbf{A}_0 \mathbf{z} + \mathbf{A}_{var} \mathbf{z} \quad (34)$$

where the constant matrix  $\mathbf{A}_0$  and the variable-dependent matrix  $\mathbf{A}_{var}$  are given by:

$$\mathbf{A}_0 = \begin{bmatrix} \mathbf{O}_{2 \times 2} & \mathbf{I}_{2 \times 2} \\ -\mathbf{M}^{-1} \mathbf{K} + \mathbf{M}^{-1} \mathbf{G} & -\mathbf{M}^{-1} \mathbf{B} \end{bmatrix} \quad (35)$$

$$\mathbf{A}_{var} = \begin{bmatrix} \mathbf{O}_{2 \times 2} & \mathbf{O}_{2 \times 2} \\ \mathbf{M}^{-1} \mathbf{K}_c & -\mathbf{M}^{-1} \mathbf{B}_c \end{bmatrix} \quad (36)$$

with  $\mathbf{I}$  and  $\mathbf{O}$  being the unit and zero matrix, respectively. By using (35) and (36) the vertices  $\mathbf{A}_1$  and  $\mathbf{A}_2$  described in (26) can be calculated. The selected extreme values of the active stiffness were  $K_{c_{min}} = 1$  Nm/rad and  $K_{c_{max}} = 1000$  Nm/rad. The resultant  $\mathbf{A}_1$  and  $\mathbf{A}_2$  are used as input to the *quadstab* MATLAB function ending up in a positive definite  $\mathbf{P}$  that satisfies (27). Therefore, the system (24) is quadratically stable implying that theoretically the active stiffness  $K_c$  can vary within the above range at an infinitely fast rate of change.

## 7. Experimental results

To evaluate this case study experiments were conducted during sit-to-stand and stand-to-sit movement with the same subject who participated in the calibration procedure described in Section 3. The subject was firstly instructed to stand up from a sitting posture while wearing the exoskeleton on his right leg and having attached the EMG electrodes to his thigh (see Fig. 13). The second task involved sitting-down from a standing posture. During the execution of the experiments the subject was asked to support most of his body weight with the right leg and use his left leg mostly for maintaining the body balancing if needed. In this manner the task became more demanding but also its duration was increased. Five trials were recorded with the exoskeleton being in zero torque mode (i.e. no motion assistance) and ten trials for each task were performed, while the exoskeleton was operating under the proposed control scheme.

The minimum and maximum values of the *STI* were obtained from the minimum and maximum co-contraction of the thigh muscles of the subject before the experiment's beginning. These were then mapped to the desired stiffness range that was set from 0 to 200 Nm/rad. The suitability of this range was validated through

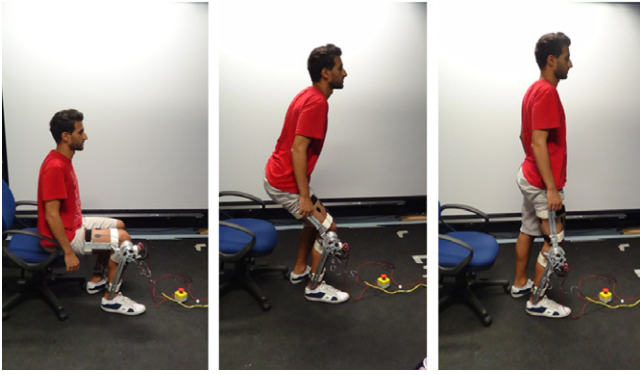


Fig. 13. Snapshots from the standing-up motion trials for experimental evaluation.

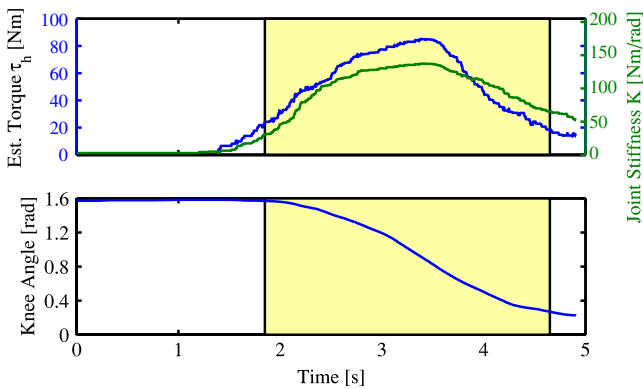


Fig. 14. A sit-to-stand trial without provided assistance; top: the estimated user’s torque, and the joint stiffness estimates. Bottom: the knee angle as recorded from the device.

a sequence of sit-to-stand and stand-to-sit trials. For all the trials, the noise dead band constant in (16) was set to  $a = 1$  Nm, while the torque integration constant  $k_f$  was experimentally tuned ensuring that the reference position update from (16) was sufficiently fast for the task execution. In particular for the standing-up was set to  $k_f = 0.034$ , whereas for the sitting-down to  $k_f = 0.045$ .

Results of one sit-to-stand trial with zero assistance are depicted in Fig. 14. The estimated user’s torque and the joint stiffness estimates, as derived from the musculoskeletal model, in addition with the knee joint position are shown. The amplitude of the user’s torque  $\tau_h$  is around 80 Nm, a value that can be confirmed also from biomechanics data in literature [46]. A quantitative evaluation of the joint stiffness estimates though is meaningless, as their values depend on the selected stiffness range.

Fig. 15 illustrates results obtained from one of the “with assistance” standing-up trials. In particular, Fig. 15(a) shows the active

stiffness of the impedance controller and the activation of each muscle. In Fig. 15(b) the assistive torque applied by the exoskeleton and the estimated user’s torque together with the trend of the knee angle  $q$  towards the equilibrium position  $\theta_{ref}$  are depicted. In all figures the phase of the standing-up motion is marked with a yellow background for convenience of the reader. As expected, the user’s torque in Fig. 15 is smaller than the one in Fig. 14, fact that highlights the received by the exoskeleton assistance. Similar reduction is observed also at the amplitude of the stiffness estimates. Moreover, the user’s torque in Fig. 15(b) exhibits a lesser degree of smoothness that justifies the human–exoskeleton interaction during the assistance. Similar findings have been reported also in [32].

In the lower plot in Fig. 15 the equilibrium position  $\theta_{ref}$  pulls via the virtual impedance the knee angle  $q$  towards the final position (standing). However, these quantities are not equal at the end of the task. This is due to the imperfect tuning of the sensitivity constant  $k_f$ , which does not perfectly fit to the time execution of the task. Future study will examine the effects of the constant  $k_f$  to the assistive functionality of the proposed system as well as possible improved methods for its tuning.

Looking at Fig. 15(a), the variation of the active stiffness follows the trace of the subject’s muscle stiffness. As expected, at free seated posture the stiffness is approximately zero. As the subject gets prepared to perform the motion his muscle activation increases and therefore the stiffness increases as well even prior to the initiation of standing (see time interval  $1.2\text{ s} < t < 2.45\text{ s}$ ). As it can be seen the standing motion begins at a knee joint stiffness of about 30 Nm/rad at  $t = 2.45\text{ s}$ . When the task initiates, the reference stiffness keeps on increasing because the subject needs to accelerate and compensate the gravitational torque. Hence, the assistive torque provided by the exoskeleton can be naturally increased. The peak of the reference stiffness occurs at  $t = 4.3\text{ s}$  when the sum of all the antagonistic muscle torques is maximum (see (10)), while the applied torque reaches its peak at  $t = 4.1\text{ s}$  according to (15). In the final phase of the task (when the subject is close to the standing posture) the muscle activation decreases (gravitational load decreases) and consequently the reference stiffness and the provided assistive torque reduce. At the standing posture the stiffness presents a constant value due to the straight knee singular position where the antagonistic muscle activation is not zero. However, this can be observed also in the case of the user’s torque indicating a limitation of the model’s prediction.

Similarly, one of the stand-to-sit trials with the exoskeleton assistance is depicted in Fig. 16. The motion task lasts for  $t = 1.65 - 4.27\text{ s}$  and is marked with a yellow background. At the standing posture the active stiffness has a low value due to the knee singular position and starts increasing when the motion begins at  $t = 1.65\text{ s}$ , see Fig. 16(a). Hence, it allows the exoskeleton to provide an assistive torque with a peak of 25 Nm to the subject

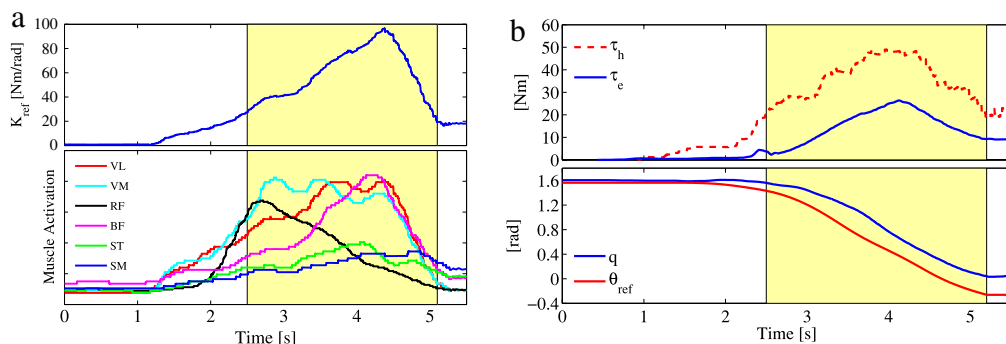
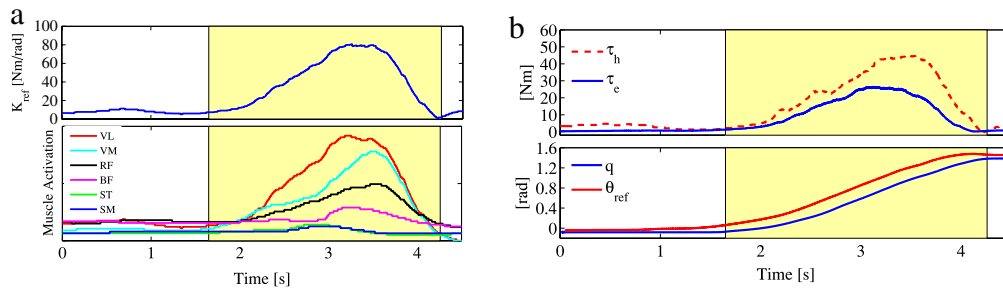


Fig. 15. (a) Active stiffness of the tele-impedance controller during standing up based on the trace of the user’s joint stiffness and the muscle activations of the six muscles. (b) Top: the applied torque by the exoskeleton and the estimated user’s torque. Bottom: the reference position (equilibrium) and the actual position of the knee exoskeleton device.



**Fig. 16.** (a) Active stiffness of the tele-impedance controller during stand-to-sit assistance and the muscle activations of the six muscles. (b) Top: the applied torque by the exoskeleton and the estimated user's torque. Bottom: the reference position (equilibrium) and the actual position of the knee exoskeleton device.

who is decelerating against gravity, see Fig. 16(b). At the end of the motion ( $t = 4.27$  s) the active stiffness is zero resulting in zero assistance. In addition, as shown in Fig. 16(b), the knee angle  $q$  moves towards the equilibrium position  $\theta_{ref}$  and reaches a constant value. Note that, the values of the active stiffness, estimated user's torque and applied torque are very comparable with the ones of the trial of the standing-up assistance shown in Fig. 15. However, as for the subject is difficult to obtain the exact sharing of weight between his two legs during the stand-to-sit and sit-to-stand trials, slight differences there can be noticed.

Furthermore, the results presented in Figs. 15 and 16 demonstrate also the advantage of the proposed control technique over simple torque amplification methods, where the assistive torque is proportional to the user's estimated torque [6,32]. The applied torques by the exoskeleton are significantly smoother, which means that the human–exoskeleton interaction and the comfort have been substantially improved [32]. In addition, this technique is more robust to unavoidable inaccuracies of the user's torque, and can provide low levels of support for small muscle activations and higher assistance for greater forces from the user, instead of performing this just proportionally with a constant ratio regardless the level of the muscle activation [32]. On the other hand, our method requires that we provide with position trajectories.

## 8. Discussion

The main evident result of the experiments is that the exoskeleton combined with the proposed control scheme can provide a large part of the required torque for standing-up. To our knowledge there is no study with regard to classification of assistance levels provided by an exoskeleton. Hence, we have assumed that the percentage of about 30% of the user's torque (i.e. the applied assistive torque in the presented experiment) is sufficient to justify the effectiveness of the exoskeleton assistance. If this is required though, the exoskeleton is able to apply greater levels of assistance by increasing the desired stiffness range (to which the stiffness trend index (STI) is mapped) and/or by adjusting the sensitivity constant  $k_f$ .

However, a matter that cannot be illustrated in figures is related to the wearer's degree of comfort, and the sense of his controllability over the device. In particular, the subject reported a seamless integration between the user intent and the operation of the exoskeleton, in addition to the experiencing of an exceedingly high degree of comfort and agility during motion. The user could receive flexible support by the exoskeleton, which he was able to regulate according to his muscle activations.

Another important issue that needs discussion regards the adopted stiffness estimation approach. As it is described in Section 5, we select to linearly map the stiffness trend index to a desired task-related and subject-specific stiffness range (see (10) and (11)). This assumption was sufficient in our setup, as the goal in this work is to replicate the stiffness trends of the human to the exoskeleton, rather than quantify joint stiffness.

Regarding defects of the proposed control technique that require improvement, the adjustment of the sensitivity constant  $k_f$  needs enhancement as it has to be carefully tuned according to the time execution of the task. Future work will examine automated methods to facilitate the derivation of the equilibrium position.

The complexity of the musculoskeletal model imposes the need for the calibration of  $7 \times n$  parameters, with  $n$  being the number of muscles. This renders the use of the device time consuming and inconvenient. A potential improvement can be accommodated through introduction of the muscle synergies [50], which gives evidence to the fact that specific motor patterns can be extracted from dominant muscles involved in the task. This requires further investigation on the contribution of the coordinated muscular activations to the task values. Moreover, the model has been calibrated in quasi-static movements where the inertia moments effect has been neglected. Future work will focus on model identification methods that will take into account inertia loads during dynamic conditions.

Furthermore, it is worth to mention that the quadratic stability of the proposed control technique has been investigated and proved that theoretically the active stiffness  $K_c$ , that is derived directly from the muscle activity of the operator, can vary at an infinitely fast rate of change.

## 9. Conclusion

This work discussed a tele-impedance based assistive control strategy for a compliant knee exoskeleton to achieve volitional stiffness augmentation and effective motion assistance, that are based on the flexibility of the user's joint. An EMG-driven musculoskeletal model, that combines results of other biomechanical works, was developed to determine the user's intended motion and the joint stiffness estimates. This model provides the reference signals to the proposed controller that allows the exoskeleton to generate assistive torques under the user's command and simultaneously exhibit high levels of transparency when no assistance is required. In addition, simulation studies of the closed-loop human–exoskeleton system were conducted and its stability was proved in both steady state and transient condition. Experimental evaluation of the proposed control strategy was carried out during the standing-up and sitting-down demonstrating that the user was able to volitionally and intuitively control the knee exoskeleton while receiving an effective motion assistance.

Future work will seek to enhance the model and its calibration method to achieve faster, more convenient use with the exoskeleton. In addition, experimentation will be extended with disabled individuals with limited leg torques in order to verify the suitability of this control method in such conditions.

## Appendix A. Supplementary data

Supplementary material related to this article can be found online at <http://dx.doi.org/10.1016/j.robot.2014.09.027>.

## References

- [1] H. Kazerooni, A. Chu, R. Steger, That which does not stabilize, will only make US stronger, *Int. J. Robot. Res.* 26 (1) (2007) 75–89.
- [2] J.F. Veneman, R. Kruidhof, E.E.G. Hekman, R. Ekkelenkamp, E.H.F. Van Asseldonk, H. van der Kooij, Design and evaluation of the LOPES exoskeleton robot for interactive gait rehabilitation, *IEEE Trans. Neural Syst. Rehabil.* 15 (3) (2007) 379–386.
- [3] N. Vitiello, T. Lenzi, S. Roccella, S.M.M. De Rossi, E. Cattin, F. Giovacchini, F. Vecchi, M.C. Carrozza, NEUROExos: A powered elbow exoskeleton for physical rehabilitation, *IEEE Trans. Robot.* 29 (1) (2013) 220–235.
- [4] P. Beyl, M. Van Damme, R. Van Ham, R. Versluys, B. Vanderborght, D. Lefeber, An exoskeleton for gait rehabilitation: prototype design and control principle, in: *Robotics and Automation, 2008. ICRA 2008. IEEE International Conference on*, IEEE, 2008, pp. 2037–2042.
- [5] K. Kong, D. Jeon, Design and control of an exoskeleton for the elderly and patients, *IEEE/ASME Trans. Mechatronics* 11 (4) (2006) 428–432.
- [6] A. Tsukahara, R. Kawanishi, Y. Hasegawa, Y. Sankai, Sit-to-stand and stand-to-sit transfer support for complete paraplegic patients with robot suit HAL, *Adv. Robot.* 24 (11) (2010) 1615–1638.
- [7] REX Bionics. [www.rexbionics.com](http://www.rexbionics.com).
- [8] J.E. Pratt, B.T. Krupp, C.J. Morse, S.H. Collins, The RoboKnee: an exoskeleton for enhancing strength and endurance during walking, in: *Robotics and Automation, 2004. Proceedings. ICRA '04. 2004 IEEE International Conference on*, vol. 3, 2004, pp. 2430–2435.
- [9] R.J. Farris, H.A. Quintero, M. Goldfarb, Preliminary evaluation of a powered lower limb orthosis to aid walking in paraplegic individuals, *IEEE Trans. Neural Syst. Rehabil. Eng.* 19 (6) (2011) 652–659.
- [10] M. Grün, U. Konigorski, Observer based method for joint torque estimation in active orthoses, in: *Mathematical Modelling*, vol. 7, 2012, pp. 199–204.
- [11] T. Lenzi, S.M.M. De Rossi, N. Vitiello, M.C. Carrozza, Intention-based EMG control for powered exoskeletons, *IEEE Trans. Biomed. Eng.* 59 (8) (2012) 2180–2190.
- [12] W. Hassani, S. Mohammed, H. Rifa, EMG based approach for wearer-centered control of a knee joint actuated orthosis, in: *Intelligent Robots and Systems (IROS), 2013 IEEE/RSJ International Conference on*, 2013, pp. 990–995.
- [13] E. Guizzo, H. Goldstein, The rise of the body bots, *Spectrum*, *IEEE* 42 (10) (2005) 50–56.
- [14] H. Lee, N. Hogan, Investigation of human ankle mechanical impedance during locomotion using a wearable ankle robot, in: *2013 IEEE International Conference on Robotics and Automation, IEEE*, 2013, pp. 2651–2656.
- [15] P.H. Chang, S.H. Kang, Stochastic estimation of human arm impedance under nonlinear friction in robot joints: a model study, *J. Neurosci. Methods* 189 (2010) 97–112.
- [16] N.L. Tagliamonte, F. Sergi, G. Carpino, D. Accoto, E. Guglielmelli, Design of a variable impedance differential actuator for wearable robotics applications, in: *2010 IEEE/RSJ International Conference on Intelligent Robots and Systems, 2010*, pp. 2639–2644.
- [17] E.C. Martinez-Villalando, H. Herr, Agonist-antagonist active knee prosthesis: a preliminary study in level-ground walking, *J. Rehabil. Res. Dev.* 46 (3) (2009) 361–373.
- [18] T.C. Bulea, R. Kobicic, C.S. To, M.L. Audu, J.R. Schnellenberger, R.J. Triolo, A variable impedance knee mechanism for controlled stance flexion during pathological gait, *IEEE/ASME Trans. Mechatronics* 17 (5) (2012) 822–832.
- [19] J.A. Blaya, H. Herr, Adaptive control of a variable-impedance ankle-foot orthosis to assist drop-foot gait, *IEEE Trans. Neural Syst. Rehabil.* 12 (1) (2004) 24–31.
- [20] S. Lee, Y. Sankai, Power assist control for walking aid with HAL-3 based on EMG and impedance adjustment around knee joint, in: *Intelligent Robots and Systems, 2002. IEEE/RSJ International Conference on*, vol. 2, 2002, pp. 1499–1504.
- [21] R. Rieneer, L. Lunenburger, S. Jezernik, M. Anderschitz, G. Colombo, V. Dietz, Patient-cooperative strategies for robot-aided treadmill training: first experimental results, *IEEE Trans. Neural Syst. Rehabil.* 13 (3) (2005) 380–394.
- [22] S. Hussain, S.Q. Xie, P.K. Jamwal, Adaptive impedance control of a robotic orthosis for gait rehabilitation, in: *IEEE Transactions on Systems, Man, and Cybernetics, Part B (Cybernetics)*, 2012, pp. 1–10.
- [23] M. Garabini, A. Passaglia, F. Belo, P. Salaris, A. Bicchi, Optimality principles in stiffness control: The VSA kick, in: *2012 IEEE International Conference on Robotics and Automation, IEEE*, 2012, pp. 3341–3346.
- [24] N. Karavas, A. Ajoudani, S.J., N. Tsagarakis, A. Bicchi, C. D G, Tele-impedance based stiffness and motion augmentation for a knee exoskeleton device, in: *Robotics and Automation, 2013. IEEE International Conference on*, 2013.
- [25] T.S. Buchanan, D.G. Lloyd, K. Manal, T.F. Besier, Neuromusculoskeletal modeling: estimation of muscle forces and joint moments and movements from measurements of neural command, *J. Appl. Biomech.* 20 (4) (2004) 367.
- [26] T.S. Buchanan, D.A. Shreeve, An evaluation of optimization techniques for the prediction of muscle activation patterns during isometric tasks, *J. Biomech. Eng.* 118 (1996) 565.
- [27] F.E. Zajac, Muscle and tendon: properties, models, scaling, and application to biomechanics and motor control, *Crit. Rev. Biomed. Eng.* 17 (4) (1989) 359.
- [28] C. De Luca, The use of surface electromyography in biomechanics, *J. Appl. Biomech.* 13 (1997) 135–163.
- [29] D.G. Lloyd, T.F. Besier, An EMG-driven musculoskeletal model to estimate muscle forces and knee joint moments in vivo, *J. Biomech.* 36 (6) (2003) 765–776.
- [30] A.V. Hill, The heat of shortening and the dynamic constants of muscle, *Proc. Roy. Soc. Lond. Ser. B, Biological Sciences* 126 (843) (1938) 136–195.
- [31] M. Sartori, M. Reggiani, E. Pagello, D.G. Lloyd, Modeling the human knee for assistive technologies, 2012.
- [32] C. Fleischer, G. Hommel, A Human-exoskeleton interface utilizing electromyography, *IEEE Trans. Robot.* 24 (4) (2008) 872–882.
- [33] P.A. Huijting, Important experimental factors for skeletal muscle modelling: non-linear changes of muscle length force characteristics as a function of degree of activity, *Eur. J. Morphol.* 34 (1) (1996) 47–54.
- [34] J.J. Visser, J.E. Hoogkamer, M.F. Bobbert, P.A. Huijting, Length and moment arm of human leg muscles as a function of knee and hip-joint angles, *Eur. J. Appl. Physiol.* 61 (5) (1990) 453–460.
- [35] K.N. An, K. Takahashi, T.P. Harrigan, E.Y. Chao, Determination of muscle orientations and moment arms, *J. Biomech. Eng.* 106 (1984) 280.
- [36] R. Osu, D.W. Franklin, H. Kato, H. Gomi, K. Domen, T. Yoshioka, M. Kawato, Short-and long-term changes in joint co-contraction associated with motor learning as revealed from surface EMG, *J. Neurophysiol.* 88 (2) (2002) 991–1004.
- [37] J.F. Veneman, R. Ekkelenkamp, R. Kruidhof, F.C.T. van der Helm, H. van der Kooij, A series elastic- and bowden-cable-based actuation system for use as torque actuator in exoskeleton-type robots, *Int. J. Robot. Res.* 25 (3) (2006) 261–281.
- [38] G. Pratt, M. Williamson, Series elastic actuators, in: *Proceedings 1995 IEEE/RSJ International Conference on Intelligent Robots and Systems*, in: *Human Robot Interaction and Cooperative Robots*, vol. 1, IEEE Comput. Soc. Press, 1995, pp. 399–406.
- [39] N.C. Karavas, N.G. Tsagarakis, J. Sgaglia, D.G. Caldwell, A novel actuator with reconfigurable stiffness for a knee exoskeleton: Design and modeling, in: J.S. Dai, M. Zoppi, X. Kong (Eds.), *Advances in Reconfigurable Mechanisms and Robots I*, Springer, London, 2012, pp. 411–421.
- [40] N.C. Karavas, N.G. Tsagarakis, D.G. Caldwell, Design, modeling and control of a series elastic actuator for an assistive knee exoskeleton, in: *Biomedical Robotics and Biomechanics (BioRob), 2012 4th IEEE RAS EMBS International Conference on*, 2012, pp. 1813–1819.
- [41] T. Lenzi, N. Vitiello, S.M.M. De Rossi, S. Roccella, F. Vecchi, M.C. Carrozza, NEUROExos: A variable impedance powered elbow exoskeleton, in: *2011 IEEE International Conference on Robotics and Automation, 2011*, pp. 1419–1426.
- [42] R. Schiavi, G. Grioli, S. Sen, A. Bicchi, VSA-II: a novel prototype of variable stiffness actuator for safe and performing robots interacting with humans, in: *2008 IEEE International Conference on Robotics and Automation, 2008*.
- [43] A. Ajoudani, N. Tsagarakis, A. Bicchi, Tele-impedance: Teleoperation with impedance regulation using a body-machine interface, *Int. J. Robot. Res.* 31 (13) (2012) 1642–1656.
- [44] A. Ajoudani, N.G. Tsagarakis, A. Bicchi, Tele-impedance: Towards transferring human impedance regulation skills to robots, in: *International Conference of Robotics and Automation - ICRA 2012*, Saint Paul, MN, USA, 2012.
- [45] N. Hogan, Impedance control: An approach to manipulation: Part III-Applications, *J. Dyn. Syst. Meas. Control* 107 (1985) 17–24.
- [46] A. Kralj, R.J. Jaeger, M. Muni, Analysis of standing up and sitting down in humans: definitions and normative data presentation, *J. Biomech.* 23 (11) (1990) 1123–1138.
- [47] L.-Q. Zhang, G. Nuber, J. Butler, M. Bowen, W.Z. Rymer, In vivo human knee joint dynamic properties as functions of muscle contraction and joint position, *J. Biomech.* 31 (1) (1997) 71–76.
- [48] L. Grman, D. Rosinova, A. Kozakova, V. Vesely, Robust stability conditions for polytopic systems, *Int. J. Syst. Sci.* (2005) 1–20.
- [49] A. Trofino, C.E.D. Souza, Biquadratic stability of uncertain linear systems, *IEEE Trans. Autom. Control* 46 (8) (2001) 1303–1307.
- [50] A. D'Avella, P. Saltiel, E. Bizzi, Combinations of muscle synergies in the construction of a natural motor behavior, *Nature Neurosci.* 6 (3) (2003) 300–308.



**Nikos Karavas** received the Dipl.-Eng. degree in Electrical and Computer engineering from the University of Patras, 2009. In 2014 he obtained the Ph.D. degree in the field of Human-centered mechatronics at the Advanced Robotics Department of the Italian Institute of Technology. Currently, he is a Postdoctoral Researcher at the Harvard Biodesign Lab of the Harvard University. He received the Best Student Paper award at ROBIO 2013. His research interests include among others: assistive wearable robotics, variable impedance systems, biomechanics and control of compliant robots.



**Arash Ajoudani** received Ph.D. degree from Centro “E Piaggio”, University of Pisa, and Humanoids and Human Centred Mechatronics Lab, Advanced Robotics Department (ADVR), Italian Institute of Technology (IIT), in 2014. He is currently a postdoctoral researcher at the ADVR, IIT. He was a winner of the best student paper award at ROBIO 2013, and a finalist for the Best Manipulation paper award at ICRA 2012. He is currently serving as a Co-Chair for the Student Activities Committee (SAC) of the IEEE Robotics and Automation Society (RAS). His main research interests are in physical human-robot interaction, impedance control, rehabilitation robotics, robust and adaptive control, and tele-robotics.



**Nikos Tsagarakis** received the Dip.-Eng. degree in electrical and computer science engineering from the Aristotle University in Greece, in 1995, the M.Sc. degree in control engineering in 1997, and the Ph.D. degree in robotics from the University of Salford, Salford, UK, in 2000. Before becoming a Senior Researcher at Italian Institution of Technology, Genova, Italy, with over-all responsibility for Humanoid and Human Centred Mechatronics Design, he was a Research Fellow and then a Senior Research Fellow in the Centre for Robotics and Automation at the University of Salford, where he worked on haptic

systems, wearable exoskeletons, rehabilitation robots, and humanoid robots. He is the author or coauthor of more than 140 papers in research journals.



**Jody Saglia** received the B.Eng. degree in automation engineering and the M.Sc. degree in mechatronics engineering from the Polytechnic of Turin, Turin, Italy, in 2004 and 2007, respectively, and the Ph.D. degree from King's College London, London, UK, in 2010. He was a researcher at King's College London in 2006. Since 2007, he has been a Research Fellow at the Istituto Italiano di Tecnologia, Genova, Italy, where he is currently a Researcher at the Rehab Technologies Facility. His research interests include mechanisms design, rehabilitation robotics, mechatronic design, actuation systems, and human–robot interaction.

Dr. Saglia received the Professional Engineering Publishing Award from the Journal of Systems and Control Engineering in 2009.



**Antonio Bicchi** is Professor of Robotics at the University of Pisa, and Senior Scientist at the Italian Institute of Technology in Genoa. He graduated from the University of Bologna in 1988 and was a postdoc scholar at M.I.T. Artificial Intelligence lab in 1988–1990. His main research interests are in Robotics, Haptics, and Control Systems in general. He has published more than 300 papers on international journals, books, and refereed conferences. He currently serves as the President of the Italian Association of Researchers in Automatic Control. He has served as Editor in Chief of the Conference Editorial Board for the IEEE Robotics and Automation Society (RAS), as Vice President and as Distinguished Lecturer of IEEE RAS. He is Editor-in-Chief for the book series “Springer Briefs on Control, Automation and Robotics”, and is in the editorial board of several scientific journals, including the top-ranked Int.J. Robotics Research, the IEEE Trans. on Robotics and Automation, IEEE Trans. Automation Science and Engineering, and IEEE RAS Magazine.



**Darwin Caldwell** received the B.S. and Ph.D. degrees in robotics from the University of Hull, Hull, UK, in 1986 and 1990, respectively and the M.Sc. degree in management in 1996 from the University of Salford, Salford, UK. He is currently the Director of Advanced Robotics at the Italian Institute of Technology, Genova, Italy, and a Visiting/Honorary Professor at the Universities of Sheffield, Manchester, Kings College, Bangor, and Tianjin (China). He is the author or coauthor of more than 300 academic papers, and has 15 patents. His research interests include innovative actuators, force augmentation exoskeletons, dexterous manipulators, humanoid (iCub and COMAN) and quadrupled robots (HyQ), and rehabilitation robotics.

Dr. Caldwell received the Professional Engineering Publishing Award from the Journal of Systems and Control Engineering in 2009.